Nuclear Instruments and Methods 196 (1982) 87–96
North-Holland Publishing Company

RECENT DEVELOPMENTS OF LIQUID XENON DETECTORS

Tadayoshi DOKE

Science and Engineering Research Laboratory, Waseda University, Kikuicho-17, Shinjuku-ku, Tokyo, Japan

The present status of the liquid xenon detector recently developed in Japan and its future plans are described. Firstly, some of the physical constants and operational properties of liquid xenon as a detector medium are mentioned. Next, the performances of several types of liquid xenon detectors which have already been built and tested are presented and finally, some possible future plans are discussed.

1. Introduction

Liquid xenon is expected to be a promising detector medium for the detection of gamma-rays, because of its high atomic number, its high atomic density and the high mobility of the electrons in it. Since the latter half of the 1960s, when the high electron mobility in liquid xenon was discovered, trials for the application of liquid xenon to nuclear radiation detectors have been made by several investigators. In the early 1970s, Derenzo's group at LBL found that electron multiplication occurs in liquid xenon [1] and, in the middle of the 1970s, Lansiart's group at Saclay found that photon multiplication, called "proportional scintillation", also occurs in liquid xenon as well as in the gaseous state [2]. Recently, we have systematically investigated the characteristics of proportional scintillation in liquid xenon and have found that they are similar to those in rare gases [3,4]. These findings mean that we can use liquid xenon with almost the same modes as those in gaseous detectors. Namely, liquid xenon can possibly be used as a position sensitive detector as well as a gamma-ray spectrometer from the analogy with the gaseous X-ray detectors. Also, liquid xenon can be used as a detector medium with multiwire drift chambers for minimum ionizing particles or, with calorimeters for high energy gamma-rays or electrons. Until now, however, these practical applications have not been made. Nevertheless, we expect that the use of liquid xenon will open a new field of nuclear radiation detectors. It seems likely that the remaining difficulties to be overcome are mainly technical ones. We are at present attempting to produce a practical liquid xenon detector.

In this paper, we first describe the fundamental properties of liquid xenon as a detector medium. We then describe the performance of the liquid xenon detectors constructed and tested by our group so far and finally present some new plans considered to be possible in the near future.

2. Fundamental properties of liquid xenon as a detector medium

The fundamental properties of liquid xenon as a detector medium are shown in table 1. Here, let us compare these properties with those of NaI(Tl) crystal or gaseous xenon.

The atomic number is slightly larger than the effective atomic number (~ 50) of NaI(Tl), but its density is smaller than that (3.76 g/cm^3) of NaI(Tl) by 16%. As a result, the detection efficiency for gamma-rays is estimated to be comparable with, or, slightly larger than that of NaI(Tl). On the other hand, the energy resolution in the ionization mode, estimated from the W-value and the Fano factor in the table, is very close to that of a Ge(Li) detector [6]. Also, the drift velocity of electrons in liquid xenon at high electric field is not so different from that in the gaseous state. For these reasons, liquid xenon is expected to be a gamma-ray spectrometer with good energy resolution and with a large detection efficiency comparable with that of the NaI(Tl) detector. Also, the radiation length of liquid xenon is almost the same as that (2.56 cm) of NaI(Tl). This means that a compact sized calorimeter with better energy resolution than that of a NaI(Tl) crystal calorimeter is possible.

In addition, the electron drift velocity is nearly constant in an electric field higher than 3 kV/cm. Recently the diffusion coefficients of electrons in liquid argon and xenon have been measured by our group and, as expected, their values are much smaller than those in gases. From these properties, it is clear that liquid xenon is suitable as a detector medium for a position sensitive detector.

In table 1 the properties of liquid xenon for the operational modes such as proportional scintillation and proportional ionization also are shown. In the proportional ionization mode, the gain of electron multiplication is considerably smaller than that in the gaseous state (as can be seen in table 1) and its operation is not

0029-554X/82/0000–0000/$02.75

Table 1
Physical properties of liquid xenon as a detector medium

		Ref. no.
Operation temperature (K)	170–185	
Operation pressure (atm)	1.5–3.0	
Density (g/cm^3)	~3	
Atomic number	54	
Radiation length (cm)	2.6	
W-value (eV)	15.6±0.3	[5]
Fano-factor	(0.041, 0.059)	[6]
Low field electron mobility (cm^2 s^{-1} V^{-1})	2000±200	[7]
Saturation velocity of electrons (cm s^{-1})	$2.6\times10^5\pm10\%$	[8]
Threshold energy of electron multiplication (V cm^{-1})	$1-2\times10^6$	[9]
Maximum charge gain	200	[9]
Threshold energy of proportional scintillation (V cm^{-1})	$4.0-7.0\times10^5$	[4]
Maximum photon gain for 20 μm wire at 5 kV (number of photons per electron)	~5	[4]
Diffusion coefficient of electrons (cm^2 s^{-1})	50–80	[10]

so stable. We found that the energy resolution deteriorates with an increase of the applied voltage [9]. So, it is not suitable as a gamma-ray spectrometer, but its signals can be used as timing signals. On the other hand, the proportional scintillation mode is stable and can also produce fast signals. Furthermore, it is expected that as high a resolution of position as well as of energy will be achievable for gamma-rays as in a gas proportional scintillation counter for X-rays [11].

3. Present status of liquid xenon detector developments

Until now, several types of liquid xenon detectors have been constructed and tested by our group for studying the fundamental properties of liquid xenon as a detector medium and for applying a liquid xenon detector to practical use. Here, we would like to summarize these experiences from the viewpoints mentioned above.

3.1. Small parallel plate chamber [10,12]

In a drift chamber, the spread of electrons due to diffusion in the drift space is one of the most fundamental limiting factors for determining the incident position of radiation. To measure the diffusion coefficient of electrons in liquid xenon, we constructed a small parallel plate chamber, which is a kind of Townsend's apparatus. The collector, which has an area of 24×24 mm^2, consists of sixteen gold strips of 20 μm in width with a spacing of 10 μm and two outer electrodes of 12 mm in width, evaporated on a ceramic plate. In this experiment, electrons produced in liquid xenon by alpha-particles emitted from a ^{210}Po source of 1 mm in length and less than 20 μm in width, deposited on the cathode surface, were used as an electron source. The spread of the electrons becomes wider during drifting from the cathode to the collector, and finally they are collected by strip collectors. From the charge distribution on the strip collectors thus obtained, we can estimate the diffusion coefficients of electrons in liquid xenon. Fig. 1 shows the variation of the latter versus electric field as well as the results for liquid argon. The value of the diffusion coefficient for liquid xenon is about $\frac{1}{50}$ lower than that for gaseous xenon and is small enough to suppress the fluctuation of the center of

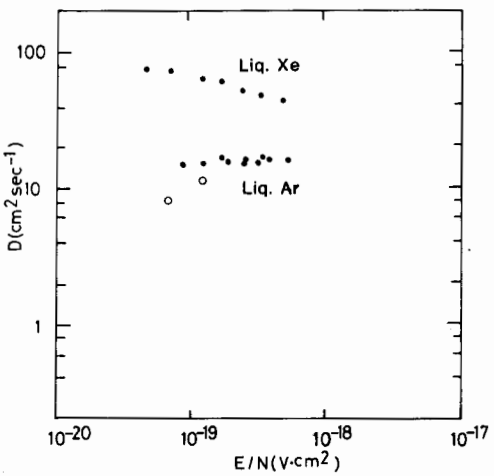

Fig. 1. Diffusion coefficients of electrons in liquid xenon and argon versus the density-normalized electric field. The full circles represent the authors' results and the open circles the results obtained by Derenzo [LBL, Group A Physics Note No. 786 (1974) unpublished].

gravity of the electron charge distribution of less than 1 μm for a drift distance of 2 mm.

3.2. Gridded ionization chamber

3.2.1. Small chamber [5]

To measure the W-value in liquid xenon, we used a small gridded ionization chamber, consisting of two circular stainless disks of 17 mm diameter used as collector (C) and cathode (K), and a grid placed between them. The arrangement of these electrodes is shown in the insert in fig. 2. The grid is an array of gold-plated stainless steel wires of 11.5 μm diameter, strung with a 150 μm spacing onto a flange and its shielding inefficiency is estimated to be 1.88% [13].

A typical pulse height spectrum obtained from a ^{207}Bi source put on the cathode surface is shown in fig. 2. This spectrum is remarkably different from that observed by a silicon detector or a liquid argon chamber. Namely, the ordinary pattern shows the peaks of K conversion electrons to be larger than those of L conversion electrons, but in liquid xenon, the situation is reversed. This fact is due to the larger photoelectric absorption coefficient of liquid xenon for gamma-rays. In particular, the main part of the peak near 550 keV comes from the photoabsorption of gamma-rays of 569 keV. Accordingly, its peak is suitable for an analysis of the energy resolution for gamma-rays. The variation of the energy resolution for gamma-rays of 569 keV with electric field is shown in fig. 3, as well as the level of electronic noise. The energy resolution (fwhm) at high electric field is 6–7%, which is about twice the noise level. It seems that the applied electric field is still not

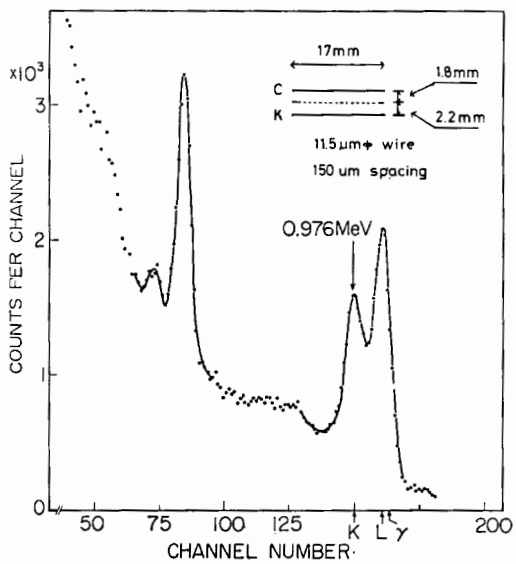

Fig. 2. A typical pulse height distribution of ^{207}Bi obtained by a small liquid xenon gridded chamber.

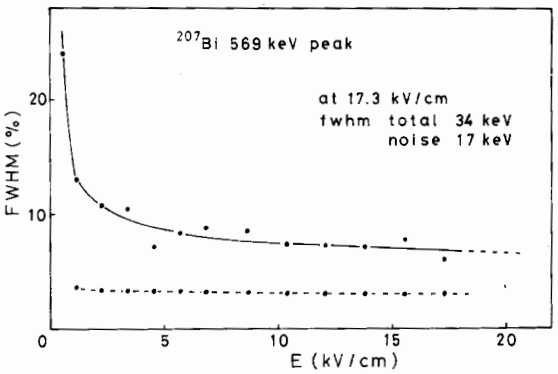

Fig. 3. The variations of the energy resolution for gamma-rays of 569 keV for the electric field.

high enough to obtain better energy resolution, because it still improves with an increase of the electric field. However, the results shown in fig. 3 mean that an energy resolution of at least 34 keV is achievable with an electric field of ~ 17 kV/cm. Recently, Obodovsky and Pokachalov obtained an energy resolution of 45 keV for 662 keV gamma-rays with an electric field of 9.5 kV/cm by using a small gridded ionization chamber [14]. This result is in good agreement with that estimated from the curve of energy resolution versus electric field shown in the figure.

3.2.2. Large chamber [15]

Recently, we constructed a dual-type gridded ionization chamber with a sensitive volume of 2 × (13 mm in depth × 50 mm in diameter), a cross-section of which is shown in fig. 4. This chamber consists of two sets of gridded ionization chambers, each of which has a collector, a grid and a common cathode. In order to obtain a higher electric field using the same applied voltage, the distances between the grid and the cathode and between the collector and the grid were changed to be 10.5 mm and 2.5 mm, respectively. The grids are arrays of gold-plated tungsten wires of 10 μm diameter, strung with a spacing of 150 μm onto a gold plated-flange of tungsten alloy and the shielding inefficiency of the grid is estimated to be 0.9% for the ordinary arrangement and 1.5% for the special arrangement for high electric field. The electrode system is suspended in the stainless steel vessel at the upper part of the cryostat by four glass feedthroughs which are fixed at the top flange of the cryostat as shown in the figure. Negative high voltage was supplied to the cathode and the grids through the glass feedthroughs. According to our experience, the baking conditions of the chamber and the vessel strongly affect its performance as a spectrometer, especially when in operation for long periods of time. The baking condition used in the experiments described here is as follows: firstly, the chamber and vessel were baked at

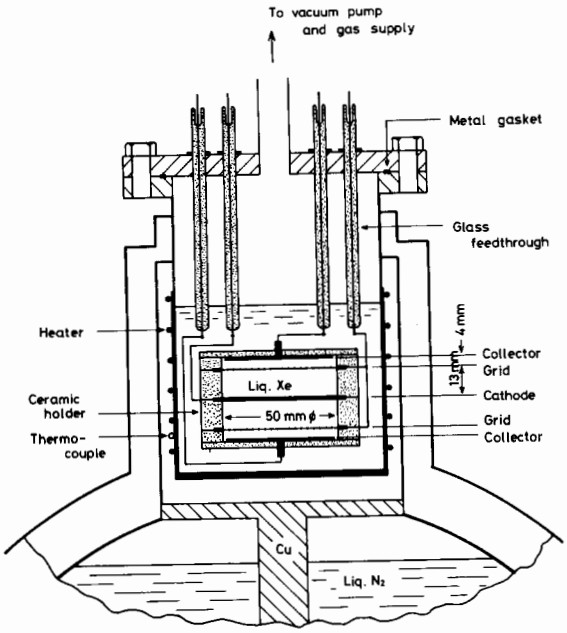

Fig. 4. A cross-sectional drawing of a dual type liquid xenon gridded ionization chamber.

about 190°C for about 72 h, then filled with liquid xenon. After that, they were evacuated again and baked at 140°C for more than 72 h, and then the xenon gas was liquefied into them for the experiment. The ultimate vacuum at room temperature was less than 5×10^{-7} Torr and the outgassing rate was less than 1×10^{-7} Torr l/s. The temperature of the vessel and the liquid xenon was maintained by liquid nitrogen in the cryostat and the heater surrounding the outside of the vessel wall. By this method, the temperature of liquid xenon was kept constant within ± 1°C.

Fig. 5 is a typical pulse height spectrum obtained by collimated gamma-rays from ^{137}Cs at an electric field of 6.5 kV/cm. The energy resolution is 8.6% fwhm for a

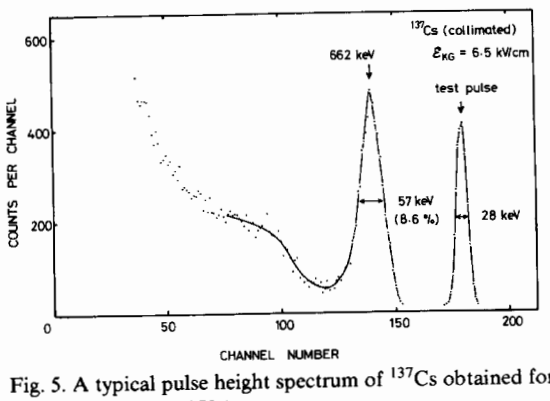

Fig. 5. A typical pulse height spectrum of ^{137}Cs obtained for an electric field of 6.5 kV/cm.

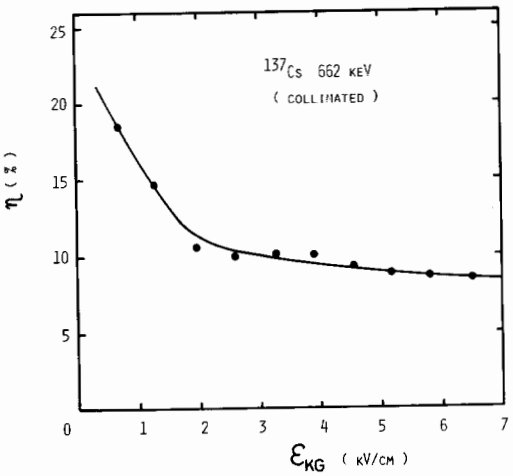

Fig. 6. The variation of the energy resolution (fwhm) with the electric field.

photoelectric peak of 662 keV. This resolution is worse than that obtained at the same electric field by the small chamber. This discrepancy cannot be attributed to electron attachment, because attenuation of collected charge could not be observed even for the drift distance of 1 cm. Fig. 6 shows the variation of energy resolution versus applied electric field. The energy resolution (fwhm) becomes still better with an increase of the electric field and it seems that the extrapolation of the resolution to higher electric field results in the same energy resolution as obtained by the small chamber. In fig. 7, the square of the energy resolution obtained with this chamber is plotted as a function of the reciprocal of the gamma-ray energy $1/E_\gamma$ as well as the curve for a conventionally available NaI(Tl) crystal of $1\frac{3}{4}''$ diameter

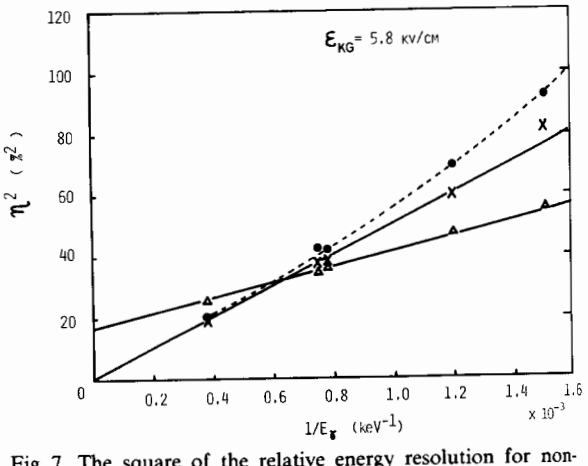

Fig. 7. The square of the relative energy resolution for non-collimated gamma-rays versus the reciprocal of the gamma-ray energy $1/E_\gamma$. The full circles are for liquid xenon; crosses, after noise correction; and open triangles, for NaI(Tl).

$\times 2''$. As can be seen from the figure, the energy resolution in liquid xenon is better than that in NaI(Tl) for gamma-rays of energy higher than 1500 keV. If an energy resolution of $\lesssim 40$ keV, as obtained by the small chamber, is achieved by increasing the applied electric field, the energy resolution of the liquid xenon detector will be superior to that of the NaI(Tl) detector over the whole energy region.

3.3. *Proportional scintillation counter* [4]

For studying the fundamental properties of proportional scintillation in liquid xenon, we used an experimental apparatus as shown in fig. 8. The electrode assembly consists of a source electrode (S), the cathode of the proportional counter (K) and its center wire (W). The source electrode is a tungsten mesh of 20 mm $\times$ 30 mm with a transparency of about 85%. The ^{207}Bi source is deposited on a stainless steel plate of about 2 mm in diameter at the center of the source electrode. The cathode is a rectangular box without an upper face. As the center wire of the proportional counter, a tungsten wire of either 4, 6, 8.5, 10, 11 or 20 μm in diameter was used. The scintillation was viewed by a photomultiplier through a 8 mm thick Pyrex glass window. Sodium salicylate of about 2 mg/cm^2 thickness was coated on the glass surface as a wavelength shifter (wls). During the experiment, the source electrode was grounded ($V_s = 0$ V), the cathode was kept at $+4$ kV ($V_k = 4$ kV) and a voltage, V_w, higher than that of the cathode was applied to the center wire. These voltages gave an electric field of about 5–8 kV/cm between the source electrode and the cathode depending on the voltage of the center wire. In such a region of electric field strength, most of the electrons are free from recombination with ions.

The pulse width of the primary scintillation observed in this experiment was about 50 ns fwhm and the pulse width of the proportional scintillation was observed to be about 200–600 ns, depending on the range and the emission angle of the conversion electrons. The best resolution of the proportional scintillation, which is not so good compared with that obtained by the liquid xenon gridded ionization chamber, is almost the same as that of the charge and it did not depend on the wire diameter. The limit of the resolution seems to be caused mainly by imperfect collection of electrons on the center wire. This is due to the fact that the size of the counter used is small compared with that necessary for perfect

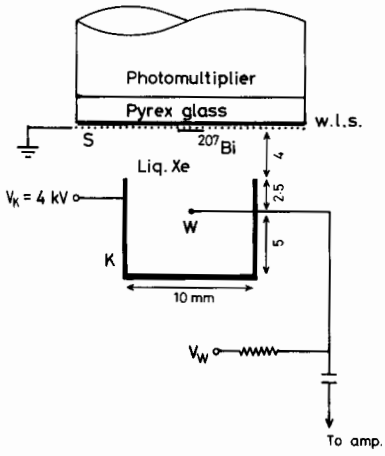

Fig. 8. Schematic cross-section of a liquid xenon proportional counter.

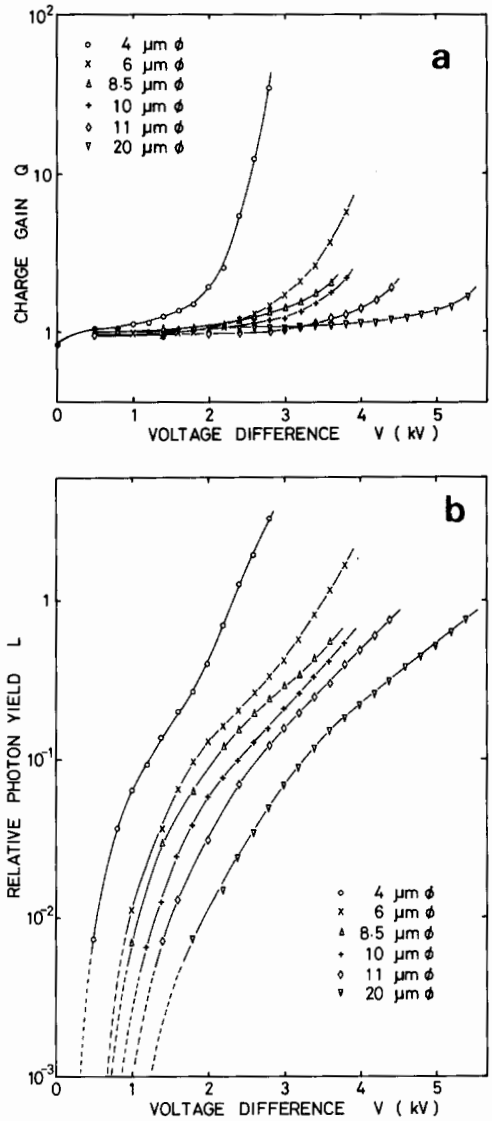

Fig. 9. (a) Charge gain Q for center wires of different diameters against $V = V_w - V_k$. (b) Relative photon yield of proportional scintillation L against V.

charge collection on the center wire when the range of electrons and size of the source are taken into consideration. Figs. 9a and b show the variation of the charge gain Q and relative photon yield L in proportional scintillation, respectively, versus the voltage difference $V = V_w - V_k$ for the 1 MeV peak of ^{207}Bi for several center wires with different diameters. In fig. 9a, the plateaus correspond to the saturation region in the ionization mode and the increase of the charge gain at a higher voltage means the beginning of the electron avalanche. The electron avalanche begins at $V \simeq 1.5$ kV for the center wire of 4 μm in diameter and $V \simeq 5$ kV for the center wire of 20 μm in diameter, which corresponds to an electric field of $1 \sim 2 \times 10^6$ V/cm at the surface of the center wire. From an analysis of the data given in fig. 9b, we found that the increase in relative photon yield with applied voltage in liquid xenon can be partly explained by the linear relation between the photon yield and the electric field strength for the production of photons in liquid xenon ($4 \sim 7 \times 10^5$ V/cm) is nearly equal to the value calculated by considering liquid xenon as gaseous xenon at 520 atm. The number of photons emitted by one electron in the proportional scintillation process is estimated to be about five for a 20 μm wire at $V = 5$ kV, from the comparison between the photon yield of primary scintillation and that of proportional scintillation.

3.4. Single wire drift chamber

3.4.1. Small chamber [3]

In order to test the possible use of liquid xenon in a drift chamber, we constructed a simple drift chamber with a fixed electron drift space which is composed of an electrode assembly and a photomultiplier as shown in fig. 10. The electrode assembly consists of a source plate, a guide ring and a proportional counter. A ^{210}Po source of 1 mm in diameter is deposited on the central part of the source plate. A tungsten wire of 4 μm in diameter was used as the anode wire of the proportional counter and a window is open on the top side of the cathode of the proportional counter to detect proportional scintillation emitted around the anode wire. To keep the electric field uniform in the electron drift space, a square guide ring was inserted between the source plate and the proportional counter. These electrodes are arranged to give an electron drift space of 13 mm, as shown in the figure. To observe both the primary and proportional scintillations by a photomultiplier, two parts on the surface of the Pyrex glass window (just above the source and above the proportional counter) are coated by sodium salicylate as a wavelength shifter. In this experiment, the drift time of electrons produced by alpha-particles was measured by using the primary scintillation pulses as the start signal and the proportional scintillation as the stop signal. The direct observation of the proportional scintillation pulse at the output stage of the photomultiplier gives the rise time of about 100 ns.

Fig. 11 shows the variation of the spatial resolution (expressed by the r.m.s value) obtained by this apparatus for the applied anode voltage as well as that obtained by using the proportional ionization pulses as the stop signal. These spatial resolutions are obtained by assuming the electron drift velocity to be 3×10^5 cm/s. As can be seen in the figure, the resolution when using the proportional ionization pulse as a stop signal is worse than that when using the proportional scintillation pulse over the whole region of the applied anode voltage. In both cases, the resolution in the ionization region is worse than that in the electron multiplication region, but in the region of applied voltage higher than 2.8 kV, the resolution becomes worse again. Therefore, the best resolution is given at about 2.8 kV. The best value of the spatial resolution was ± 23 μm for the proportional ionization mode and ± 19 μm for the

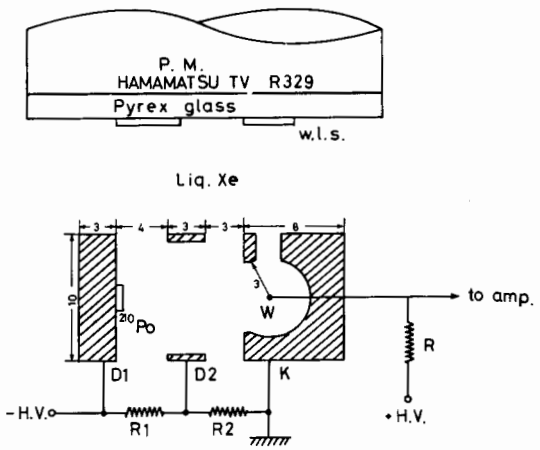

Fig. 10. Schematic cross-section of a small single wire liquid xenon drift chamber.

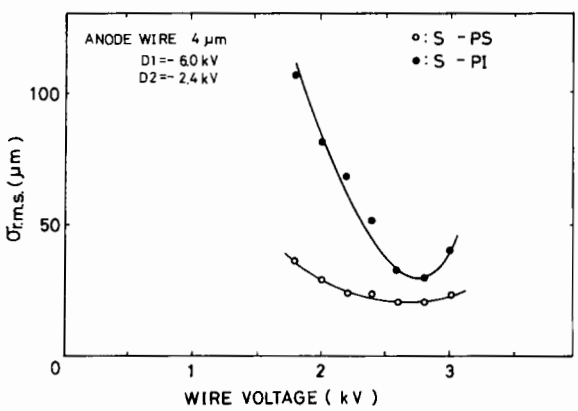

Fig. 11. Spatial resolution (r.m.s.) versus anode voltage.

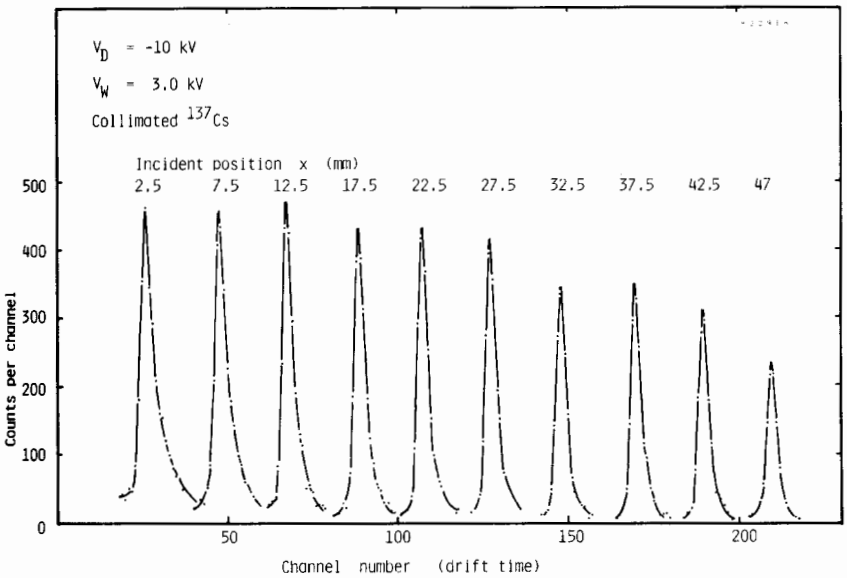

Fig. 12. Spectra of the electron drift time for various incident positions of 662 keV collimated gamma-rays, observed by a liquid xenon single wire drift chamber with a drift space of 50 mm.

proportional scintillation mode. The existence of the optimum resolution in the proportional ionization mode is explained as follows. In the ionization chamber region, the spatial resolution is poor, because of the low signal-to-noise ratio and in the higher voltage region, the rapid deterioration of spatial resolution is caused by an increase in the spread of the pulse height distribution. In the proportional scintillation mode, on the other hand, there also exists an optimum resolution but the variation of the spatial resolution with applied voltage is small, because the signal-to-noise ratio is comparatively large for the low applied voltage and the spread of the pulse height distribution in the higher voltage region is small compared with that in the proportional ionization mode. According to our analysis, the spatial resolution is mainly determined by the range effect of alpha-particles and the size effect of the alpha source. This means that if such a drift chamber is used for minimum ionizing particles, a spatial resolution of less than $\pm 10\ \mu$m can be expected, as shown later.

3.4.2. Large chamber [16]

Recently we constructed a liquid xenon single wire drift chamber with a drift space of 50 mm for measuring electron momentum in metal by using annihilation gamma-rays. This chamber consists of a drift space of electrons the sensitive volume of which is 50 mm × 50 mm × 10 mm and a single wire proportional counter for the detection of the drift electrons. The measurement of drift time was made by the same method as that used in the previous one. Fig. 12 shows the spectra of the electron drift time for various incident positions of 662 keV collimated gamma-rays, obtained using this drift chamber. As can be seen in the figure, the mean spatial resolution of 0.9 mm (fwhm) was obtained. In this measurement, the effective width of the collimated gamma-rays is estimated to be 0.56 mm. If the contribution from the beam width is subtracted from the above value, a value of about 0.6 mm will be expected as an intrinsic resolution, which is practically achievable. The details of this drift chamber have been reported by Masuda et al. [16]. Here, we describe two new findings made during the present experiment.

(a) *Attenuation length of drifting electrons.* Since this chamber has a long drift distance, precise measurements of the attenuation length of electrons in liquid xenon are possible by using collimated gamma-rays. For the measurements we used the charge spectra obtained with the ionization mode. The results for an electric field of 2 kV/cm are shown in fig. 13. The amount of the attenuation for a drift path length of 50 mm is about 5% of the initial charge at that electric field. This means that the attenuation length for electron attachment is about 1 m and shows that liquid xenon will be useful as a detector medium in the so-called "time projection chamber".

(b) *Temperature dependence of electron drift velocity.* In the course of the experiments, we found that the drift velocity of electrons in liquid xenon depends a great deal on the temperature of the liquid. In fig. 14, the time necessary for electrons to drift a distance of 50 mm is plotted versus the temperature of liquid xenon. This figure shows that the drift velocity is almost inversely proportional to the temperature of the liquid and the slope gives the change of 0.5% per °C. Such a temperature dependence cannot be neglected for the precise

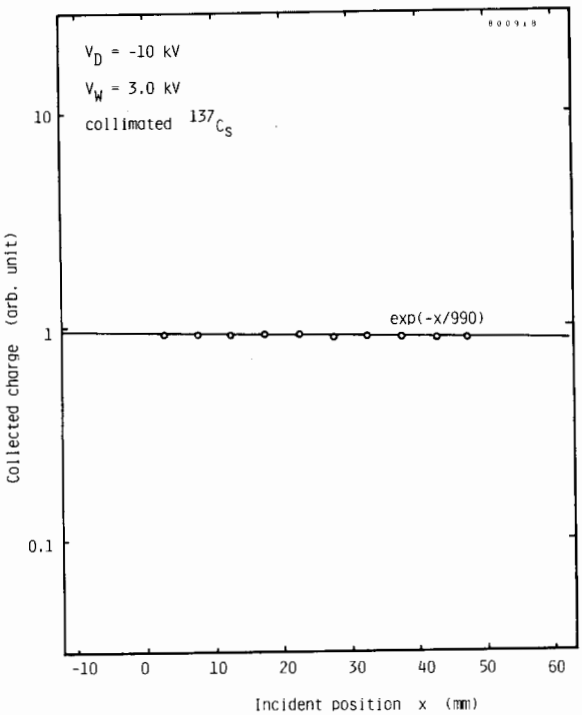

Fig. 13. The attenuation of collected charge versus the drifting distance.

measurement of position. Namely, if we aim to achieve a high spatial resolution of the order of μm by using a multiwire drift chamber, the temperature variation during the measurement must be suppressed to within ± 0.2°C.

4. New plans

In this section, we will describe some experiments actually in progress or being planned.

4.1. Gridded ionization chamber with position sensitivity

For gamma-rays, high position resolution is not required because of the long range of the electrons emitted by gamma-rays. So, we are considering the use of a simple method such as a charge division type in order to obtain a position sensitivity in a gridded ionization chamber. For example, let us consider a gridded ionization chamber with a resistive plate as a collector and use it as a two-dimensional position detector. In the charge division method, the position resolution in the one-dimensional case is given by the following formula [17,18],

$$P \simeq K(T/R)^{1/2} L/E, \quad \tau \gtrsim RC/2$$

where K is a constant; τ is the pulse shaping time constant; T is the absolute temperature; R is the resistance of the resistive electrode; C is the detector capacitance; L is the detector length; E is the energy deposition in the detector. Now, let us assume that $\tau = RC/2$, $T = 180$ K, $C = 20$ pF and $L = 100$ mm, and estimate the position resolution for 1 MeV gamma-rays. The above formula gives a resolution of about 1.8 mm. This

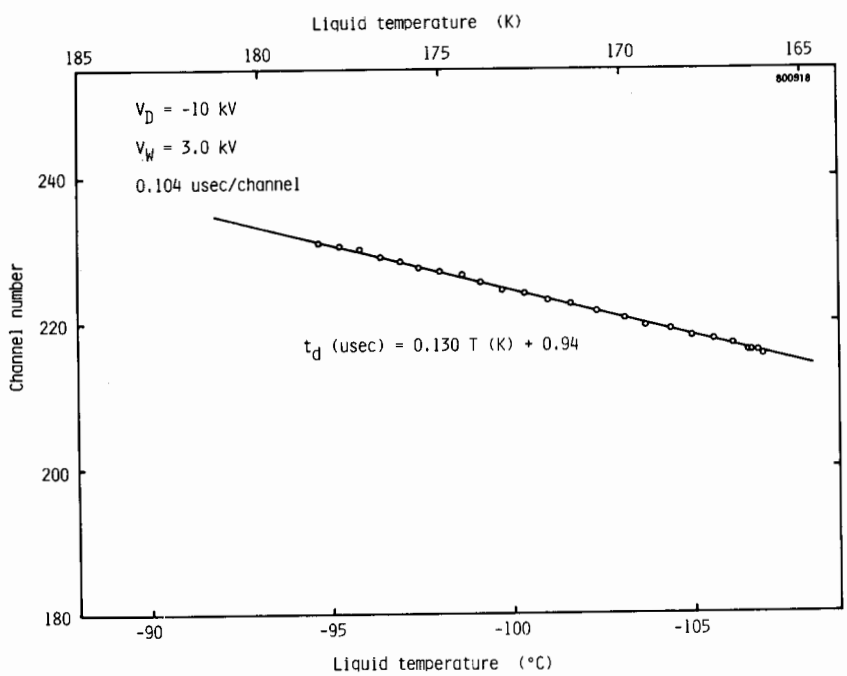

Fig. 14. Temperature dependence of electron drift velocity in liquid xenon.

is good enough to determine the incident position of 1 MeV gamma-rays, because the range of electrons emitted by the gamma-rays is of the order of a mm. If we use a resistive electrode of 10 kΩ, the value of RC is 2×10^{-7} s. So, it is possible to use a fast amplifier of the differential and integral time constants of $\tau\sim0.2$ μs, although a slow amplifier with $\tau=1$–2 μs is required for obtaining the information concerning the energy of the gamma-rays. By using such fast ionization pulses and the signals of its primary scintillation, it is also possible to measure the drift time of electrons with an accuracy of $\sim\pm0.5$ μs, corresponding to a position accuracy of $\sim\pm1.5$ mm. This means that this type of detector can be used as a kind of time projection chamber. At present, we expect that such a liquid xenon chamber will be used for the observation of cosmic gamma-rays in the near future.

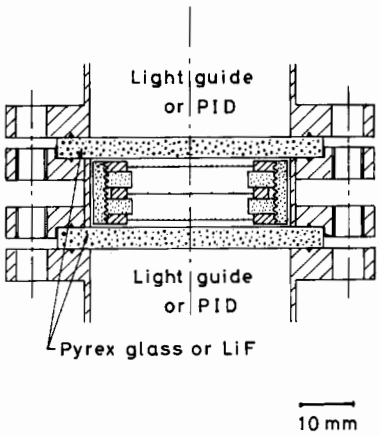

Fig. 15. Schematic cross-sectional view of a multiwire proportional scintillation chamber.

4.2. Calorimeter for high energy gamma-rays or electrons

At present, liquid argon calorimeters with converter electrodes are widely used in the field of high energy physics. The liquid argon calorimeter has a comparatively good energy resolution for high energy gamma-rays and can easily read out the three-dimensional pattern of an electron cascade shower. However, the energy resolution is worse than that of a NaI(Tl) crystal calorimeter. If a pure liquid calorimeter without converter electrodes is used, an energy resolution comparable with or better than that of a NaI(Tl) calorimeter may be achieved as expected from the results obtained with the ionization chamber mode. Because of its large radiation length, however, the size of the chamber becomes considerable. If liquid xenon, having a short radiation length, is used in place of liquid argon, a compact calorimeter with good energy resolution and position sensitivity will be realized. We are planning such a calorimeter in the form of a multiplate liquid xenon chamber, consisting of many electrodes made of very thin stainless foils, being better than the multi-cylindrical-chamber type, in which it is difficult to collect the full of electron charge because of the low electric field near the cathode surface.

4.3. Multiwire proportional scintillation chamber

In order to achieve good energy resolution for gamma-rays by using a proportional scintillation chamber, it is necessary to collect precisely all of the electrons produced by the gamma-rays and avoid the loss of light due to the wire shadow effect. To satisfy both conditions, we recently designed and constructed a kind of multiwire proportional scintillation chamber, as shown in fig. 15. At the center of the chamber, many thin wires of 10 μm in diameter are strung with 4 mm spacing with metallic meshes on both sides, 5 mm from the center, as cathodes. The proportional scintillation is viewed by two photomultipliers put on both sides. Usually, a wave length shifter is coated on the inner surface of both Pyrex glass windows. In such a design, the electric field near the cathodes is strong and the so-called shadow effect is also eliminated. If the liquid xenon photo-ionization chamber (PIC) as suggested by Policarpo [19] can be used in place of photomultipliers, and the Pyrex plass window are also replaced by LiF windows, its energy resolution will be much improved. Furthermore, if the liquid xenon PICs can be operated as position sensitive detectors, we can easily obtain two-dimensional information for incident gamma-rays. Such a chamber will be useful in the wide filed. A test experiment on this type of chamber is in progress.

4.4. Multiwire drift chamber with ultra-high position resolution

To use a liquid xenon drift chamber as a position sensitive detector for minimum ionizing particles, we designed a multiwire drift chamber arranged as shown in fig. 16 and estimated its position resolution for 3 GeV/c protons. The result is shown in table 2. In this estimation, we made the following assumptions ; (1) the center of the gravity of the charge distribution produced by a minimum ionizing particle is measured; (2) the proton passes through the following materials: 20 mm thick styro-foam, 1 mm thick copper plate, 2 mm thick ceramic plate as a base for strip cathodes and 1.5 mm of liquid xenon; (3) the maximum deviation in wire setting is ±2.5 μm; and (4) the time resolution of the circuit is 0.3 ns.

As can be seen in table 2, the ultimate spatial resolution is 4 μm, which is mainly caused by Rutherford scattering. Recently, we started to test such a liquid xenon position sensitive detector and in the near future,

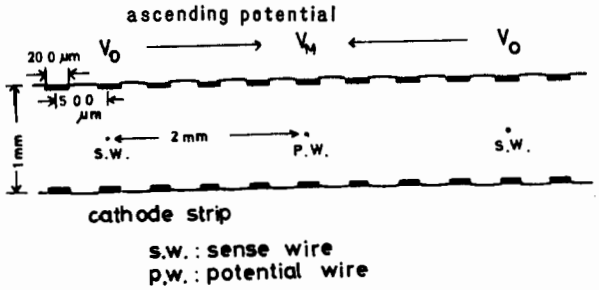

Fig. 16. The arrangement of electrodes in the multiwire drift chamber with ultra-high position resolution.

Table 2
Estimation of position resolution in a liquid xenon multiwire chamber

Diffusion of electrons	0.6 μm
Fluctuation of primary ionization	less than 1 μm
Multiple coulomb scattering	3.8 μm
Sense wire arrangement	0.7 μm
Contribution from electronic circuit	0.9 μm
Total	4.0 μm

an experiment on minimum ionization particles will be performed at KEK.

References

[1] R.A. Muller, S.E. Derenzo, G. Smadja, D.B. Smith, T.G. Smits, H. Zaklad and L.W. Alvarez, Phys. Rev. Lett. 27 (1971) 532.
[2] A. Lansiart, A. Seigneur, J. Moretti and J. Morucci, Nucl. Instr. and Meth. 135 (1976) 47.
[3] M. Miyajima, K. Masuda, Y. Hoshi, T. Doke, T. Takahashi, T. Hamada, S. Kubota, A. Nakamoto and E. Shibamura, Nucl. Instr. and Meth. 160 (1979) 239.
[4] K. Masuda, S. Takasu, T. Doke, T. Takahashi, A. Nakamoto, S. Kubota and E. Shibamura, Nucl. Instr. and Meth. 160 (1979) 247.
[5] T. Takahashi, S. Konno, T. Hamada, M. Miyajima, S. Kubota, A. Nakamoto, A. Hitachi, E. Shibamura and T. Doke, Phys. Rev. A12 (1975) 1771.
[6] T. Doke, A. Hitachi, S. Kubota, A. Nakamoto and T. Takahashi, Nucl. Instr. and Meth. 134 (1976) 353.
[7] K. Yoshino, U. Sowada and W.F. Schmidt, Phys. Rev. A14 (1976) 438.
[8] E. Shibamura, A. Hitachi, T. Doke, T. Takahashi, S. Kubota and M. Miyajima, Nucl. Instr. and Meth. 131 (1975) 249.
[9] M. Miyajima, K. Masuda, A. Hitachi, T. Doke, T. Takahashi, S. Konno, T. Hamada, S. Kubota, A. Nakamoto and E. Shibamura, Nucl. Instr. and Meth. 134 (1976) 403.
[10] E. Shibamura, T. Takahashi, S. Kubota and T. Doke, Phys. Rev. A20 (1979) 2547.
[11] A.J.P.L. Policarpo, M.A.F. Alves, M.C.M. dos Santos and M.J.T. Carvalho, Nucl. Instr. and Meth. 102 (1972) 337.
[12] E. Shibamura, S. Kubota, T. Takahashi and T. Doke, Proc. Int. Seminar on Swarm Experiments in Atomic Collision Research, Tokyo (1979) p. 47.
[13] O. Bunneman, J.E. Cranshow and J.A. Harvey, Can. J. Res. 27 (1949) 191.
[14] I.M. Obodovsky and S.G. Pokachalov, Low Tem. Phys. 5 (1979) 829.
[15] K. Masuda, A. Hitachi, Y. Hoshi, T. Doke, A. Nakamoto, E. Shibamura and T. Takahashi, Nucl. Instr. and Meth. 174 (1980) 439.
[16] K. Masuda, T. Doke and T. Takahashi, Nucl. Instr. and Meth. 188 (1981) 629.
[17] J.L. Alberi and V. Radeka, IEEE Trans. Nucl. Sci. NS-23 (1976) 251.
[18] A. Doehring, S. Kalbitzer and W. Helzer, Nucl. Instr. and Meth. 59 (1968) 40.
[19] A.J.P.L. Policarpo, these Proceedings, p. 53.